PROCEEDINGS OF SCIENCE

Herschel and PEP resolve the far-IR background

Stefano Berta*, **Benjamin Magnelli, Raanan Nordon, Dieter Lutz & the PEP Team**
Max Planck Institut für Extraterrestrische Physik
E-mail: berta@mpe.mpg.de

The cosmic infrared background (CIB) is studied taking advantage of the PACS 70, 100, 160 μm observations of the GOODS-N, GOODS-S, Lockman Hole and COSMOS fields, belonging to the PACS Evolutionary Probe (PEP) survey. We produce number counts covering more than two orders of magnitude in flux, from $\sim$1 mJy to few hundreds mJy. Stacking of 24 μm sources and $P(D)$ statistics extend the analysis down to the sub-mJy regime. The available ancillary information allows number counts to be split into redshift bins. At $z \leq 0.5$ we isolate a class of luminous IR galaxies ($L_{IR} \sim 10^{11}$ L$_{\odot}$), whose SEDs peak at $\sim$130 μm restframe, thus significantly colder than what is expected on the basis of the local luminosity-temperature relation. The integral of number counts provides an estimate of the CIB surface brightness of $\nu I_{\nu} = 3.61 \pm 1.12$, 8.04 ± 1.39 and 8.84 ± 1.11 [nW m^{-2} sr^{-1}] at 70, 100, and 160 μm, respectively. These correspond to 56 ± 10% and 70 ± 9% of the direct CIB measurements at 100 and 160 μm. Employing the $P(D)$ analysis, these fractions increase to $\sim$60% and $\sim$82%. Most of this resolved CIB fraction was radiated at $z \leq 1.0$, with redder sources lying at higher redshift than blue ones.

Cosmic Radiation Fields: Sources in the early Universe - CRF2010,
November 9-12, 2010
Desy Germany

*Speaker.

PoS(CRF 2010)001

1. Introduction

With the exception of the cosmic microwave background, which represents the relic of the Big Bang, the extragalactic background light (EBL) from γ-rays to radio frequencies is the integral of the energy radiated by all galaxies, across all cosmic epochs. The optical and infrared backgrounds dominate the EBL by several orders of magnitude with respect to all other spectral domains. In this budget, the cosmic infrared background (CIB), detected for the first time by COBE [1, 2], accounts for roughly half of the total EBL (e.g. [3]; see [4] for a review).

The deep extragalactic campaigns carried out in the nineties and 2000's with the *Infrared Space Observatory* (ISO, see [5] for a summary), and *Spitzer Space Telescope* ([6]; e.g. [7]) resolved most of the EBL in the mid-IR (15 and 24 μm) into individual sources. On the contrary, at wavelengths where the CIB peaks — between 100 and 200 μm — the performance of these telescopes was strongly limited by their small apertures ($\sim$ 85 cm diameter), the prohibitive confusion limits, and the sensitivity of detectors. Past surveys produced only limited samples of distant far-IR objects (e.g. [8]): in the 160 μm Spitzer/MIPS band $\sim$ 7% of the CIB was resolved into individually detected objects [9], and only stacking of 24 μm sources actually allowed to retrieve most of the far-IR CIB [3, 10].

Launched in May 2009, Herschel [11] is providing stunning results: thanks to the favourable diffraction limit of its large 3.6 m mirror, and the high sensitivity of its *Photodetector Array Camera & Spectrometer* (PACS, performing imaging at 70, 100, 160 μm; [12]) confusion and blending of sources are much less of a limitation. It is now possible to resolve the majority of the CIB peak into individual galaxies.

Here we exploit data from the *PACS Evolutionary Probe* (PEP[1]) extragalactic survey, in order to build far-IR number counts, and derive the amount of CIB resolved by Herschel. PEP covers the most popular and widely studied extragalactic blank fields and is structured as a "wedding cake" survey. Its tiers include the wide (2 deg^2) and shallow COSMOS field, medium depth areas like the Lockman Hole, EGS and ECDFS, pencil-beam very deep observations of GOODS-N and GOODS-S, and ten nearby lensing clusters (e.g. Abell 2218), offering the chance to break the PACS confusion limit thanks to gravitational lensing. Our survey is complementary to the other ongoing Herschel extragalactic campaigns: HerMES ($\sim$70 deg^2, [13]) including most of SWIRE [14] wide fields and observing with both PACS and SPIRE ([15], 250, 350, 500 μm) instruments; ATLAS [16] covering 550 deg^2; H-GOODS, reaching the confusion limit at 100 μm in a subset of the GOODS fields [17]; and the Herschel Lensing Clusters survey [18]. We defer to [19] and [20] for an in depth description of the PEP survey.

2. PEP number counts

Here we make use of the GOODS-N, GOODS-S ($\sim$150 arcmin^2), Lockman Hole ($\sim$ 450 arcmin^2) and COSMOS ($\sim$2 deg^2) areas observed by PEP, thus covering different flux regimes and different field sizes (see [20, 31]). In addition, early results based on the lensing cluster Abell 2218 [32] are briefly summarized.

[1] http://www.mpe.mpg.de/ir/Research/PEP/

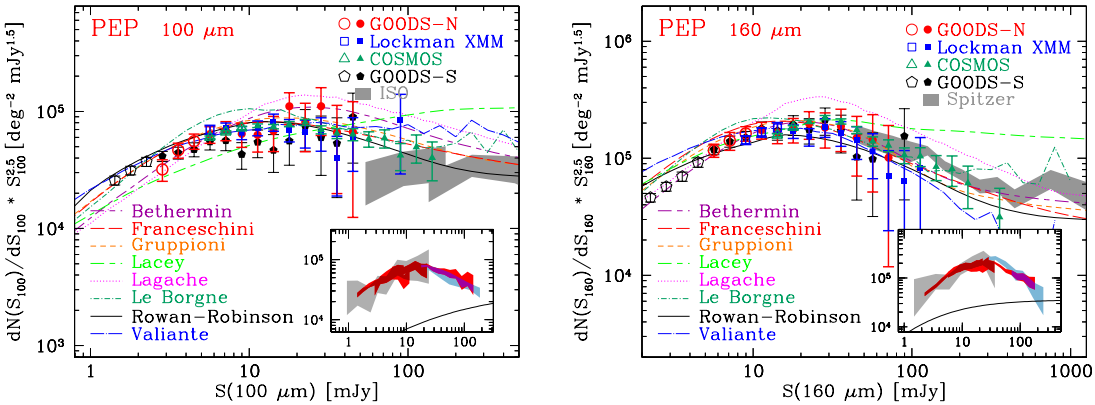

Figure 1: Number counts at 100 (*left*) and 160 μm (*right*), normalized to the Euclidean slope. Filled/open symbols belong to flux bins above/below the 80% completeness limit. Models belong to [21 – 28]. Shaded areas represent ISO and Spitzer data [29, 30, 10]. *Inset*: Collection of PACS number counts, including PEP blank fields (red, [20, 31]), PEP Abell 2218 (grey, [32]) and HerMES-PACS (light-blue, [33]) The solid lines in the insets mark the trends expected for a non-evolving population of galaxies.

PACS number counts are shown in Fig. 1, normalized to the Euclidean slope ($dN/dS \propto S^{-2.5}$). Filled symbols belong to the 80% completeness limit, open symbols extend down to the 3σ level, applying completeness corrections as prescribed by [34]. Error bars include Poisson statistics, flux calibration uncertainties, and photometric errors. The 95 μm ISO counts [29, 30] and 160 μm Spitzer results [10], including GOODS/FIDEL, COSMOS and SWIRE fields) are consistent with PACS data, excepted the ISO faintest flux bin. Small insets in Fig. 1 show results from PACS Guaranteed-Time surveys.

Based on the [36, 35] mass model of Abell 2218, [32] have been able to estimate the gravitational flux amplification affecting background galaxies in the observed field. Consequently it was possible to de-boost the observed fluxes and extend the number counts down to the mJy regime, deeper than the PEP GOODS-S field. For comparison, the 16.7 src/beam confusion limit is reached at $\sim$1.5-2.0 mJy and $\sim$8.0 mJy, in the GOODS-N/S fields, at 100 and 160 μm, respectively.

Several evolutionary models are compared to the data in Fig. 1. The most successful ones are the [25] recipe, including luminosity-dependent distribution functions for the galaxy IR SEDs and their AGN contribution; the [23] model, employing analytic evolutionary functions without discontinuities and 4 galaxy populations, and the [22] solution, calling into play a population of high-redshift very luminous objects, resembling sub-mm galaxies.

3. Slicing number counts

The GOODS fields benefit from an extensive multi-wavelength coverage. Following [37], the PEP team built a reliable multi-wavelength, PSF-matched catalog in GOODS-N, including *UbvizJHK*, IRAC, MIPS 24 μm and PACS data, as well as spectroscopic and newly-computed photometric redshifts (see [20] for further details). Similarly, we took advantage of the GOODS-S MUSIC [37] multi-wavelength catalog and matched it to the available 24 μm [38] and PACS

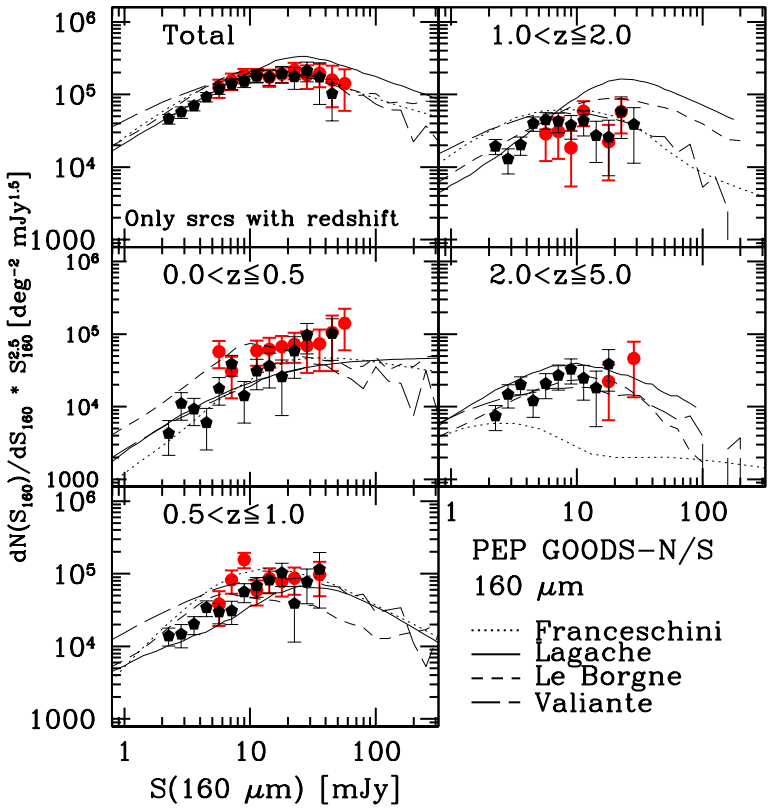

Figure 2: Slicing the PEP population into redshift bins: 160 μm differential number counts split in redshift bins. Red/black symbols belong to the GOODS-N/S fields.

data. This rich dataset allows us to split the far-IR number counts into redshift bins (Fig. 2), hence providing further constraints on the evolution of galaxy populations.

It is interesting to note that at redshift $z \leq 0.5$ the differential number counts, normalized to the Euclidean slope, monotonically increase as a function of flux, recalling the trend expected for a non-evolving population of galaxies. At the bright end, above 10-20 mJy, the observed number counts show an excess with respect to most models. This excess turns out to be stronger at 160 μm (see [20]), suggesting that these galaxies might be on average colder than those adopted in backward models. The left panel of Fig. 3 shows the results of SED fitting [39]: half of this sample shows a late-spiral SED (*Sd-Sdm* in the [40] library), with typical luminosities above 10^{11} $L_{\odot}$. The peak wavelength of these SEDs is $\sim$130 μm, while at these luminosities [41] models — which adopt the local $L-T$ relation — predict SEDs peaking around 90 μm restframe. This class of objects is indeed colder than typical local IR-luminous sources. The right-hand panel in Fig. 3 shows the SED of one typical case, with $L(IR) \sim 10^{11.3}$ $L_{\odot}$.

4. Stacking analysis

Limiting the number counts analysis to individually-detected sources only, we miss a significant fraction of the information stored in PACS maps. It is common use to adopt stacking of sources

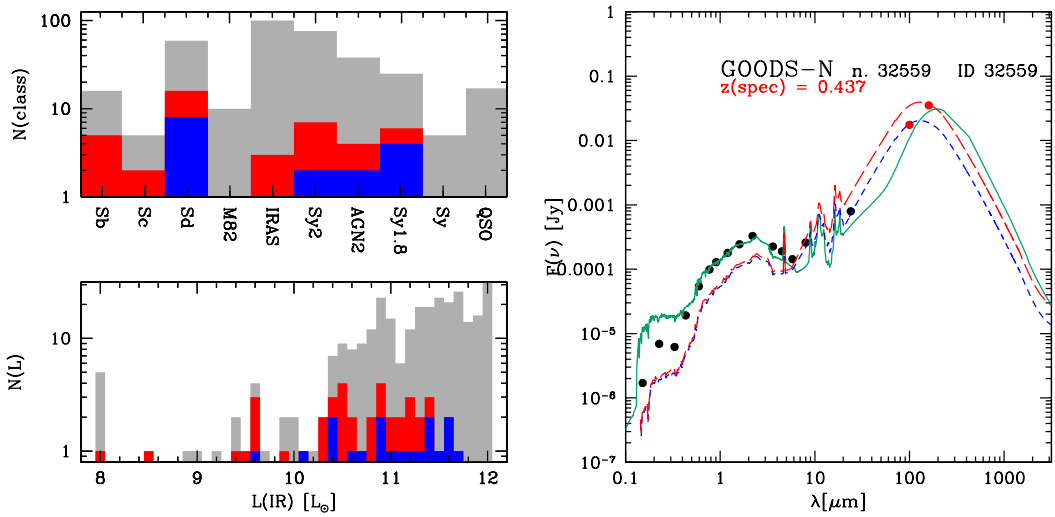

Figure 3: *Left panel*: Distribution of IR luminosities and best fit templates for the whole PACS population (grey), and for $z \leq 0.5$ galaxies with fluxes above 10 mJy (red) and 20 mJy (blue). *Right panel*: SED example of a low-redshift object with $L \sim 10^{11.3}$ $L_{\odot}$, with best fit template (green solid line) and [41] library predictions, at this luminosity and based on the 100 μm (blue, short-dash) or 160 μm (red, long-dash) observed fluxes.

from deeper data (e.g. at shorter wavelengths), or pixel statistics analyses, to extend the study of number counts and CIB to deeper flux regimes, beyond the confusion limit [3, 42, 8, 10, 43].

The 24 μm catalogs in the GOODS-S field, extending down to 20 μJy [38], provide the ideal priors to perform stacking of un-detected sources on PACS maps. With this technique we derive PACS/24μm colors as a function of 24 μm flux. The top-left panel in Fig. 4 shows the results. Stacking of mid-IR sources actually allows us to retrieve missed PACS fluxes down to faint regimes, thus recovering the actual average colors, that would not be possible to derive otherwise. Stacked points were fit with a polynomial function and then used to transform the observed 24 μm differential counts into PACS counts [31].

Although this method has been widely and successfully used by several authors, it is worth to point out that the results are affected by completeness limitations. In the specific case, a flux cut in the 24 μm priors (e.g. 20 μJy at the 3σ detection threshold) induces incompleteness in the PACS stacked fluxes, because red objects (faint at 24μm) are not included in the parent catalog. Consequently stacking of 24μm sources on the PACS maps can provide only a lower limit to the PACS number counts below a given PACS flux. Based on [24] mock catalogs, for a 24 μm cut of 20 μJy, the PACS stacked counts are 90% complete only above $\sim$0.7 mJy and $\sim$1.3 mJy at 100 and 160 μm, respectively. To this effect, one should add the intrinsic properties of the 24 μm catalog, reaching 80% completeness at $S(24) \sim 35$ μJy.

The bottom panels of Fig. 4 show the results of stacking, above the 80% stacking completeness (big blue crosses), in good agreement with the faint-end of the counts presented before (open symbols in Figs. 4 and 1).

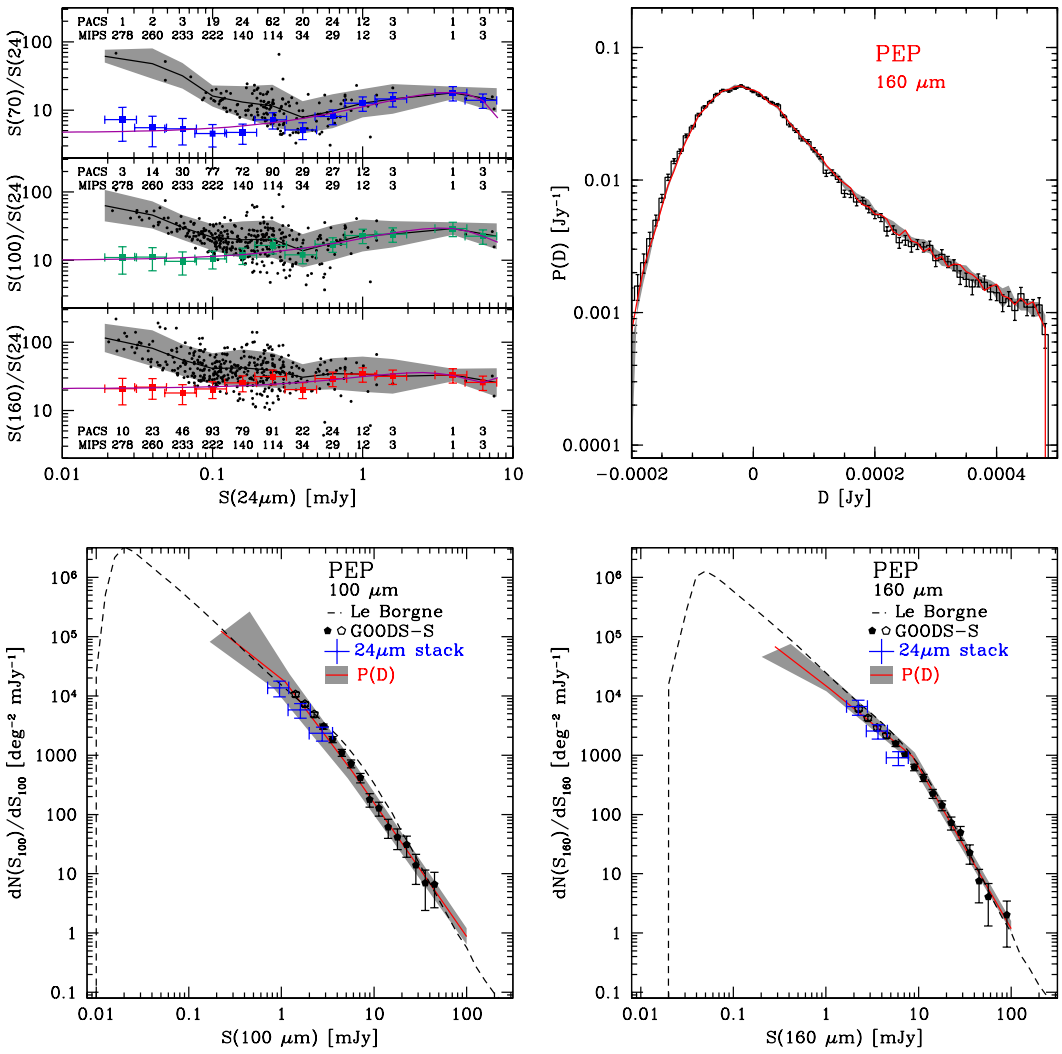

Figure 4: Stacking and $P(D)$ analyses in GOODS-S. *Top-left panel*: PACS/24μm colors of sources, as measured from individual detections (black dots) and stacking (colored symbols). The black solid lines and grey shaded areas represent average colors and dispersion of PACS-detected sources. Solid light-blue lines are polynomial fits to the stacked points. *Top-right panel*: $P(D)$ analysis at 160 μm. The black histogram and error bars belong to the observed $P(D)$, while the red solid line and grey shaded area represent the best fit and its 3σ confidence interval. *Bottom panels*: resolved differential number counts (black symbols) at 100 and 160μm, compared to the results of stacking (big blue crosses) and $P(D)$ (red solid line and 3σ grey shaded area).

5. Probability of defection

In addition to directly detected sources and to stacking of 24 μm dense catalogs, further information about the shape of PACS number counts comes from "probability of deflection" statistics, or $P(D)$ distribution [44 – 46, 22, 47, 48, 43]. In a simplified notation, this is a representation of the distribution of pixel values in a map: its shape and width are mainly driven by three components: the underlying number counts, the instrumental spatial response function (e.g. the PSF), and the

instrumental noise. If the three are known, it is possible to reproduce the observed pixel flux probability distribution, or — vice versa — the observed $P(D)$ can be used to constrain the underlying dN/dS number counts, down to flux densities not probed by other methods.

We performed the $P(D)$ analysis on PACS maps, modeling differential counts dN/dS as a broken power-law with three sections and two nodes. The position of nodes and amplitude of counts at these positions are free parameters. Minimization is carried out via a MCMC engine, reproducing the observed $P(D)$, given the counts model. The top-right panel in Fig. 4 shows the fit to the observed $P(D)$ at 160 μm [31]. The two bottom panels include the number counts model belonging to the best fit $P(D)$ (red solid line and grey shaded area). The $P(D)$ statistics allow the knowledge of PACS number counts to be extended down to $\sim$0.2 mJy. The resulting slopes are consistent with resolved and stacked counts, over the flux range in common.

6. The resolved CIB

The integral of number counts (resolved, stacked, and from $P(D)$) provides a lower limit to the cosmic IR background and can be compared to direct measurements from COBE maps (see [20, 31] for a comprehensive summary). Here we adopt the measurements by [3], who extensively describe uncertainties and calibration details: 14.4 ± 6.3 and 12.8 ± 6.4 [nW m^{-2} sr^{-1}] at 100 and 160 μm, respectively. No direct measurement is available at 70 μm, where the third PACS passband is centered, except for the [52] fluctuation analysis on the IRAS 60 μm map ($\nu I_\nu = 9.0$ [nW m^{-2} sr^{-1}]).

The contribution to the CIB of individual PEP sources is obtained by combining the number counts in GOODS-S/N, Lockman Hole and COSMOS fields, thus covering as wide a flux range as possible. The integration of number counts, including completeness corrections, gives 8.04 ± 1.39 and 8.84 ± 1.11 [nW m^{-2} sr^{-1}], corresponding to 56 ± 10% and 70 ± 9% of the direct measurements at 100 and 160 μm, respectively. The resolved CIB at 70 μm is $\nu I_\nu = 3.61 \pm 1.12$ [nW m^{-2} sr^{-1}].

Stacking of 24 μm sources provides similar values, excluding lower limits at the very faint end. Extending the analysis via $P(D)$ statistics, we recover $\sim$60% and 82% of the reference total CIB at 100 and 160 μm, already within the 1σ uncertainty of the direct measurements. Figure 5 summarizes our findings.

It is finally possible to estimate how much of the resolved CIB was emitted at different cosmic epochs. The colored histograms in Fig. 5 depicts the amount of extragalactic IR background originating from the four redshift bins taken into account in GOODS-S (see also Fig. 2). At the PEP 3σ detection threshold ($\sim$1.2 mJy at 70, 100 μm and $\sim$2.0 mJy at 160 μm), more than half of the resolved CIB is emitted by objects lying at $z \leq 1$. The relative fraction among the four bins moves from low to high redshift, as wavelength increases. While at 70 μm roughly 90% of the resolved CIB is emitted at $z \leq 1.0$, at 160 μm the CIB budget is almost equipartitioned below/above $z = 1.0$.

7. Summary

Using PACS data belonging to the PEP survey, we derived far-IR number counts in the GOODS-N/S, Lockman Hole and COSMOS fields. By employing stacking and $P(D)$ analyses, it has been

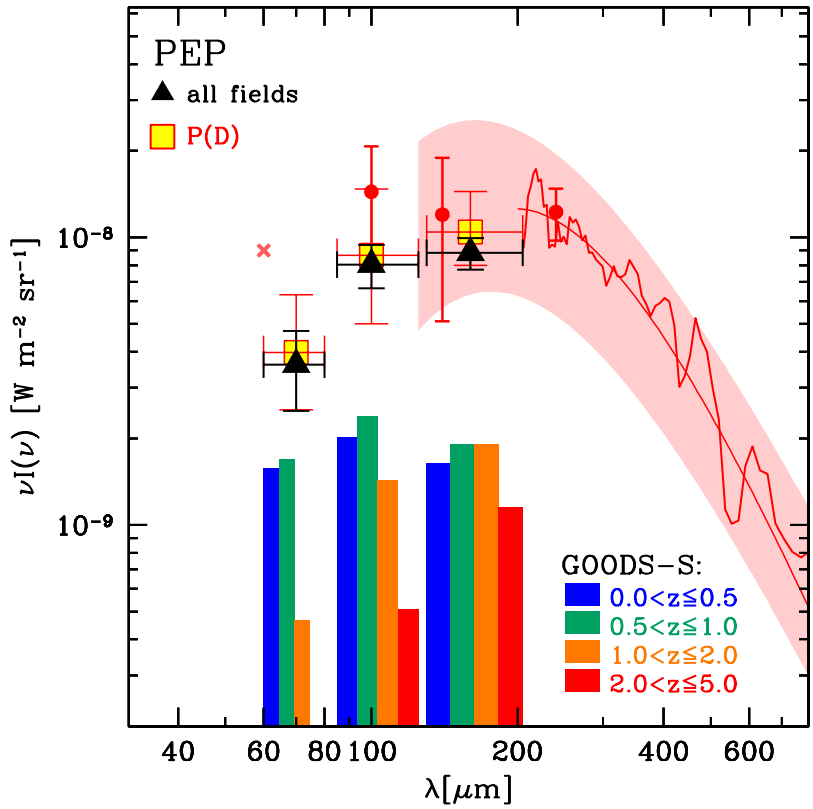

Figure 5: Contribution of PACS galaxies to the CIB [20, 31], as obtained via integration within the flux range covered by PEP. Black filled triangles belong to resolved number counts in GOODS-S/N, Lockman Hole and COSMOS, including completeness correction; yellow/red squares represent the result of the $P(D)$ analysis in GOODS-S. Histograms denote the contribution of different redshift bins to the CIB in GOODS-S. Literature data include: DIRBE measurements (filled circles, 1σ errors, [3], FIRAS spectrum (solid lines above 200 μm, [49, 50]), [51] modified Black Body (shaded area), 60 μm IRAS fluctuation analysis (cross, [52]).

possible to exploit the whole information in PACS maps and extend the study to very deep fluxes. The wealth of ancillary data in the GOODS fields allowed counts and CIB to be split into redshift bins. The integration of counts provided new, unprecedented estimates of the contribution of IR galaxies to the extragalactic background light. The main results presented here are:

- resolved far-IR number counts extend from a few mJy to $\sim$200 mJy, at 70, 100, 160 μm;
- gravitational lensing (e.g. in Abell 2218) allowed the counts to be extended down to $\sim$1.0 mJy;
- stacking and $P(D)$ analyses further improved the available information, down to a fraction of mJy in GOODS-S;
- using ancillary data in the GOODS fields, number counts and CIB have been split in redshift bins; we identify a population of cold and luminous IR galaxies at $z \leq 0.5$;

- PEP resolves 50% (70%) of the CIB at 100 μm (160 μm); using $P(D)$ statistics, this fraction increases to $\sim$60% ($\sim$82%); this is already within the 1σ uncertainty of the direct CIB measurements;
- the bulk of CIB in PACS bands was emitted at redshift $z \leq 1.0$, with the balance moving to higher redshift at longer wavelengths.

A detailed description of the PEP cosmic IR background studies can be found in [20, 31], including — among others — the full information in the three PACS bands, field-to-field variations, and finer redshift binning at low redshift.

Acknowledgements

PACS has been developed by a consortium of institutes led by MPE (Germany) and including UVIE (Austria); KU Leuven, CSL, IMEC (Belgium); CEA, LAM (France); MPIA (Germany); INAF-IFSI/OAA/OAP/OAT, LENS, SISSA (Italy); IAC (Spain). This development has been supported by the funding agencies BMVIT (Austria), ESA-PRODEX (Belgium), CEA/CNES (France), DLR (Germany), ASI/INAF (Italy), and CICYT/MCYT (Spain).

References

[1] Puget, J., Abergel, A., Bernard, J., et al. 1996, *A&A*, 308, L5+

[2] Hauser, M. G., Arendt, R. G., Kelsall, T., et al. 1998, *ApJ*, 508, 25

[3] Dole, H., Lagache, G., Puget, J., et al. 2006, *A&A*, 451, 417

[4] Hauser, M. G. & Dwek, E. 2001, *ARA& A*, 39, 249

[5] Genzel, R. & Cesarsky, C. J. 2000, *ARA& A*, 38, 761

[6] Werner, M. W., Roellig, T. L., Low, F. J., et al. 2004, *ApJS*, 154, 1

[7] Papovich, C., Dole, H., Egami, E., et al. 2004, *ApJS*, 154, 70

[8] Frayer, D. T., Sanders, D. B., Surace, J. A., et al. 2009, *AJ*, 138, 1261

[9] Dole, H., Le Floc'h, E., Pérez-González, P. G., et al. 2004, *ApJS*, 154, 87

[10] Béthermin, M., Dole, H., Beelen, A., & Aussel, H. 2010a, *A&A*, 512, 78

[11] Pilbratt, G.L., et al. 2010, *A&A*, 518, L1.

[12] Poglitsch, A., et al. 2010, *A&A*, 518, L2.

[13] Oliver, S. J., Wang, L., Smith, A. J., et al. 2010, *A&A*, 518, L21+

[14] Lonsdale, C. J., Smith, H. E., Rowan-Robinson, M., et al. 2003, *PASP*, 115, 897

[15] Griffin, M. J., et al., *A&A*, 518, L3.

[16] Eales, S., et al. 2010, *PASP*, 122, 499

[17] Elbaz, D., et al., in preparation.

[18] Egami, E., et al. 2010, *A&A*, 518, L12

[19] Lutz, D., et al. 2011, in preparation.

[20] Berta, S., Magnelli, B., Lutz, D., et al. 2010, *A&A*, 518, L30+

[21] Lagache, G., Dole, H., Puget, J., et al. 2004, *ApJS*, 154, 112

[22] Franceschini, A., Rodighiero, G., Vaccari, M., et al. 2010, *A&A*, 517, A74+

[23] Rowan-Robinson, M. 2009, *MNRAS*, 394, 117

[24] Le Borgne, D., Elbaz, D., Ocvirk, P., & Pichon, C. 2009, *A&A*, 504, 727

[25] Valiante, E., Lutz, D., Sturm, E., Genzel, R., & Chapin, E. 2009, *ApJ*, 701, 1814

[26] Lacey, C. G., Baugh, C. M., Frenk, C. S., et al. 2010, *MNRAS*, 405, 2L

[27] Béthermin, M., et al. 2010b, [astro-ph/1010.1150].

[28] Gruppioni, C., et al. 2011, in preparation.

[29] Rodighiero, G. & Franceschini, A. 2004, *A&A*, 419, L55

[30] Héraudeau, P., Oliver, S., del Burgo, C., et al. 2004, *MNRAS*, 354, 924

[31] Berta, S., et al. 2011, in preparation.

[32] Altieri, B., et al. 2010, *A&A*, 518, L17.

[33] Aussel, H., et al. 2011, in preparation.

[34] Chary, R., Casertano, S., Dickinson, M. E., et al. 2004, *ApJS*, 154, 80

[35] Kneib, J.-P., Ellis, R., Santos, M. R., Richard, J. 2004, *ApJ*, 607, 697.

[36] Kneib, J.-P., Ellis, R., Smail, I., et al. 1996, *ApJ*, 471, 643

[37] Grazian, A., Fontana, A., de Santis, C., et al. 2006, *A&A*, 449, 951

[38] Magnelli, B., Elbaz, D., Chary, R. R., et al. 2009, *A&A*, 496, 57

[39] Rodighiero, G., et al. 2010, *A&A*, 518, L25

[40] Polletta, M., Tajer, M., Maraschi, L., et al. 2007, *ApJ*, 663, 81

[41] Chary, R. & Elbaz, D. 2001, *ApJ*, 556, 562

[42] Marsden, G., Ade, P. A. R., Bock, J. J., et al. 2009, *ApJ*, 707, 1729

[43] Glenn, J., Conley, A., Bethermin, M., et al. 2010, *MNRAS*, 409, 109

[44] Scheuer, P. A. G. & Ryle, M. 1957, in Proceedings of the Cambridge Philosophical Society, Vol. 53, Proceedings of the Cambridge Philosophical Society, 764–+

[45] Condon, J. J. 1974, *ApJ*, 188, 279

[46] Franceschini, A., Toffolatti, L., Danese, L., & de Zotti, G. 1989, *ApJ*, 344, 35

[47] Oliver, S. J., Goldschmidt, P., Franceschini, A., et al. 1997, *MNRAS*, 289, 471

[48] Patanchon, G., Ade, P. A. R., Bock, J. J., et al. 2009, *ApJ*, 707, 1750

[49] Lagache, G., Abergel, A., Boulanger, F., Désert, & Puget. 1999, *A&A*, 344, 322

[50] Lagache, G., Haffner, L., Reynolds, R., & Tufte, S. 2000, *A&A*, 354, 247

[51] Fixsen, D., Dwek, E., Mather, J., Bennett, C., & Shafer, R. 1998, *ApJ*, 508, 123

[52] Miville-Deschenes, M., Lagache, G., & Puget, J.-L. 2002, *A&A*, 393, 749